Title
Concentric rings K-space trajectory for hyperpolarized 13C MR spectroscopic imaging

Journal
Magnetic Resonance in Medicine, 75(1)

ISSN
0740-3194

Authors
Jiang, Wenwen
Lustig, Michael
Larson, Peder EZ

Publication Date
2016

DOI
10.1002/mrm.25577

Peer reviewed

HHS Public Access

Author manuscript

Magn Reson Med. Author manuscript; available in PMC 2017 January 01.

Published in final edited form as:

Magn Reson Med. 2016 January ; 75(1): 19–31. doi:10.1002/mrm.25577.

Concentric Rings K-Space Trajectory for Hyperpolarized ^{13}C MR Spectroscopic Imaging

Wenwen Jiang[1], **Michael Lustig**[1,2], and **Peder E.Z. Larson**[1,3]

[1]UC Berkeley-UCSF Graduate Program in Bioengineering, University of California, Berkeley and University of California, San Francisco, California, USA

[2]Department of Electrical Engineering and Computer Sciences, University of California, Berkeley, California, USA

[3]Department of Radiology and Biomedical Imaging, University of California, San Francisco, California, USA

Abstract

Purpose—To develop a robust and rapid imaging technique for hyperpolarized ^{13}C MR Spectroscopic Imaging (MRSI) and investigate its performance.

Methods—A concentric rings readout trajectory with constant angular velocity is proposed for hyperpolarized ^{13}C spectroscopic imaging and its properties are analyzed. Quantitative analyses of design tradeoffs are presented for several imaging scenarios. The first application of concentric rings on ^{13}C phantoms and in vivo animal hyperpolarized ^{13}C MRSI studies were performed to demonstrate the feasibility of the proposed method. Finally, a parallel imaging accelerated concentric rings study is presented.

Results—The concentric rings MRSI trajectory has the advantages of acquisition timesaving compared to echo-planar spectroscopic imaging (EPSI). It provides sufficient spectral bandwidth with relatively high SNR efficiency compared to EPSI and spiral techniques. Phantom and in vivo animal studies showed good image quality with half the scan time and reduced pulsatile flow artifacts compared to EPSI. Parallel imaging accelerated concentric rings showed advantages over Cartesian sampling in g-factor simulations and demonstrated aliasing-free image quality in a hyperpolarized ^{13}C in vivo study.

Conclusion—The concentric rings trajectory is a robust and rapid imaging technique that fits very well with the speed, bandwidth, and resolution requirements of hyperpolarized ^{13}C MRSI.

Keywords

Hyperpolarized ^{13}C; Spectroscopic Imaging; Concentric Rings; Non-Cartesian Trajectory; Parallel Imaging

Address correspondence to: Peder E. Z. Larson, Ph.D. University of California - San Francisco, 1700 4th St Byers Hall, Room 102C, San Francisco, CA, USA, 94158, peder.larson@ucsf.edu.

Presented in part at the 21st and 22nd Annual Meeting of ISMRM.

Introduction

In vivo detection of ^{13}C labeled substrates by MRSI allows for observation of specific enzyme-catalyzed reactions that reflect altered metabolism in cancer [1]. This was recently made possible by creating hyperpolarized nuclear spins in the liquid state suitable for injection through a process called dissolution dynamic nuclear polarization (DNP). This process greatly improves the signal sensitivity by a factor of 10,000+ [2], thereby allowing the direct monitoring of ^{13}C metabolites in vivo as long as the data acquisition is fast enough to capture the short-lived signal (≤ 1min). The first phase I clinical trial using this technology was recently performed in the Surbeck Laboratory of Advanced Imaging at UCSF, where 31 prostate cancer patients were studied using hyperpolarized ^{13}C MRI. The study showed no adverse effect and demonstrated promising initial imaging results for detecting and staging tumors [3].

Despite these advances, the short-lived effect of hyperpolarization still poses severe challenges for imaging. It is therefore necessary to develop rapid and robust imaging techniques. Furthermore, these techniques must also resolve metabolite signals at multiple resonance frequencies. Techniques have been developed that rely on fast spectroscopic sequences that exploit the most out of the system hardware [4, 5, 6, 7, 8, 9, 10, 11], imaging-based sequences with spectral separation techniques [12, 13, 14], parallel imaging using coil arrays [15, 16, 17], and exploiting structure and redundancy in the data[18, 19] [20].

Fast spectroscopic sequences are advantageous because they provide comprehensive spectral information about all metabolites. This is especially important when using multiple hyperpolarized agents [21] or agents with more complex spectra such as [1, 2-^{13}C] pyruvate [22], which presents major design challenges for imaging-based sequences [12, 13, 14]. In comparison to these sequences, fast spectroscopic sequences are also more robust to B_0 inhomogeneities.

Currently, both Cartesian (Echo-Planar Spectroscopic Imaging or EPSI [4, 5, 23]) and non-Cartesian (spiral [7, 8, 24] and radial [6] spectroscopic imaging) techniques have been investigated for accelerated hyperpolarized ^{13}C MRSI. EPSI uses bipolar trapezoid magnetic field gradients during signal detection and offers larger k-space coverage. However it suffers from relatively long scan times due to the number of phase encodings. In addition, minor system imperfections can induce undesirable ghosting artifacts. To prevent ghosting, flyback EPSI can be used but at the expense of a more limited spectral bandwidth (SBW). This limits the number of metabolites that can be observed without aliasing. Spiral spectroscopic imaging is an alternative that provides a scan-time-efficient imaging scheme, but it is susceptible to system imperfections (such as gradient timing delay and eddy currents) [25].

To provide scan-time-efficiency and robustness to system imperfections, we propose using concentric rings trajectory (CRT) as the data acquisition method for ^{13}C MRSI. It has the following advantages: I. the acquisition time is halved compared with EPSI, given the same imaging prescriptions; II. the slew rate (a hardware limitation for magnetic field gradients) requirement is less demanding than the time-optimal spiral trajectory; III. CRT is robust to first order eddy currents and system delays; IV. this sampling trajectory results in lower g-

factor noise amplification in parallel imaging than EPSI. CRT for MRI was first proposed by Wu *et al.* [26, 27]. They implemented CRT on magnetization-prepared imaging and corrected for the off-resonance blurring by retracing the central k-space. They also analyzed the unique contrast and robustness properties of CRT. Later, Kwon *et al.* [28] implemented the concentric cylinders trajectory on 3D magnetization-prepared imaging. In their study, Kwon *et. al*, demonstrated the feasibility of the 3D concentric cylinder for magnetization-prepared imaging. In another recent work, Furuyama *et al.* [29] implemented CRT in a standard PRESS based spectroscopy sequence for proton MRSI. They demonstrated feasibility in the healthy human brain in vivo, taking advantage of the trajectory robustness and two-fold acceleration over EPSI. Quantitative comparisons between CRT and other MRSI trajectories to evaluate resolution, spectral bandwidth and SNR efficiency, have not been reported yet. Moreover, for the hyperpolarized ^{13}C MRSI application, some practical challenges and unique properties which are well-suited to CRT have not been exploited yet.

In this work, we demonstrated the efficacy of CRT through a quantitative comparison between CRT, EPSI and spiral MRSI, and used a ^{13}C MRSI CRT sequence for ^{13}C phantom and hyperpolarized ^{13}C in vivo animal applications. We also extended the application of CRT to parallel imaging for additional acceleration and analyzed noise amplification compared with Cartesian counterpart.

Methods

Concentric Rings Trajectory Design for MRSI

Our CRT for MRSI is derived similarly as in [26, 27]. Gradients are designed for the outermost ring with respect to the spatial resolution and spectral bandwidth (SBW) and then scaled down for the inner rings with the readout window $T_{readout}$ kept constant. We use CRT with constant angular velocity since they are robust to timing and eddy currents delays. The radius of the outermost ring is set according to the desired spatial resolution. Maximum gradient amplitude and slew rates set an upper limit on the achievable spectral bandwidth, which is determined by the retracing period ΔT. The number of rings N_{ring} determines the in-plane field of view (FOV), whereas the number of revolutions N_{rev} determines the spectral resolution – which is ultimately limited by T2* decay.

The prewinders and rewinders are designed using the time-optimal gradient design by Hargreaves *et al.* [30] and implemented in Matlab (The Mathworks, Natick, MA, USA.) and the CVX [31] convex optimization toolbox. The trajectory for an axial plane is shown in Figure 1.

The constant angular velocity of rings is insensitive to some system imperfections. Timing and first-order eddy currents induced delays result in benign rotations of images [27, 28] rather than spatial blurring.

Theoretical Comparison of the Concentric Rings Trajectory with EPSI and Spiral

For MRSI sequences, especially in hyperpolarized studies, optimizing the total scan time, spectral bandwidth, and SNR is crucial for capturing the intrinsic contrast and biochemical information. A quantitative study of CRT using these key parameters was performed in

order to compare against three other commonly used MRSI schemes: EPSI (both symmetric and flyback EPSI) and spiral spectroscopic trajectories. Figure 2 illustrates the k-space trajectories for the different methods. In symmetric EPSI, k-space is scanned in a zigzag trajectory and is collected in both directions (blue and yellow arrows in the symmetric EPSI in Figure 2). In our analysis we compare against a design in which the spectral bandwidth is determined by the time between scans in the same direction, such as the duration between adjacent blue arrows. This guarantees Nyquist sampling of the spectrum and is the preferred method in our institute. We refer to this approach as Nyquist-constrained symmetric EPSI [5]. However, it is possible to exploit Papoulis's generalized sampling theory [32] and double the spectral bandwidth of the current symmetric design, as it was initially implemented in proton MRSI [33]. In this situation the spectral bandwidth is defined by the time between alternate scanning directions, such as the duration between adjacent blue and yellow arrows. We refer to this approach as "critical symmetric EPSI". We elaborate on this approach in the Supporting Materials section.

For a fair comparison, we fixed some specific prescriptions when evaluating acquisition time, SBW and SNR efficiency with respect to the spatial resolution. The parameter ranges were chosen according to typical routine hyperpolarized preclinical prescriptions for [1-^{13}C]pyruvate that were performed in our institute: FOV = 16 × 16 cm^2(Here, we need to mention that CRT and spiral have circular FOV while EPSI has a square FOV, so they are not exactly identical. We defined the extent of imaging support along the x and y axes to be the FOV), spectral resolution = 10 Hz (*i.e.*, the readout window $T_{readout}$ = 100 ms), spatial resolution was in the range from 0.36 cm to 1 cm. All designs assumed a gradient amplitude limit of 40 mT/m and maximum slew rate of 150 mT/m/ms.

Acquisition Time Comparison—The acquisition time should be as short as possible to "freeze" the ^{13}C signal while hyperpolarized compounds undergo metabolic conversion and before they decay back to equilibrium. In order to compare acquisition time, we fixed the SBW = 500 Hz, TR = 200 ms, spectral resolution = 10 Hz and FOV = 16 × 16 cm^2. The total acquisition time $T_{\text{acquisition time}}$ is simply the product of TR, the number of phase encodings N_{pe} and the number of interleaves in time $N_{interleaves}$.

$$T_{\text{acquisition time}} = TR \times N_{\text{pe}} \times N_{\text{interleaves}} \quad (1)$$

SNR Efficiency Comparison—In our SNR efficiency comparisons, we fixed the following parameters: SBW = 500 Hz, spectral resolution = 10 Hz and FOV = 16 × 16 cm^2. We considered the duty cycle and the k-space sampling uniformity effects on SNR efficiency. (We did not consider T1 effects and the number of excitations. Unlike conventional imaging, hyperpolarized ^{13}C imaging often uses a progressive flip angle [34], which equalizes the magnetization for each excitation. This results in an SNR that is independent of the number of excitations and this is elaborated in the Parallel Imaging with Concentric Rings section. Since relatively small number of excitations was considered here, T1 effects could be neglected. When the acquisition is long, T1 decay during the scan will reduce the available magnetization. It is worth mentioning that spirals and rings will have the advantage over EPSI since they require fewer acquisitions.)

SNR efficiency depends on the duty cycle:

$$SNR_{\text{eff,duty}} = \sqrt{\frac{T_{\text{active time}}}{T_{\text{readout}}}}, \quad (2)$$

where $T_{\text{active time}}$ is the total duration of the active readout gradients while T_{readout} is the duration of readout window.

It is also dependent on the uniformity of the sampling trajectory. Non-uniform sampling acquisitions are less SNR efficient than uniform ones. This was nicely demonstrated in [35], where the effective SNR efficiency is given by:

$$SNR_{\text{eff,uniformity}} = \frac{A_k}{\sqrt{\int_{\vec{k}} D(\vec{k}) d\vec{k} \int_{\vec{k}} \frac{1}{D(\vec{k})} d\vec{k}}}, \quad (3)$$

where $D(\vec{k})$ is the density of the corresponding sampling position, and A_k is the k-space coverage.

We defined the overall SNR efficiency to be the product of the above two formulas and computed the SNR efficiency for different trajectories.

For flyback and symmetric EPSI, we were required to use ramp sampling (as otherwise the SBW requirement was not achievable). For the spiral trajectory, we designed time-optimal spiral trajectories for different imaging resolution in order to minimize the total acquisition time, which was essential for hyperpolarized ^{13}C imaging.

Spectral Bandwidth—Spectral bandwidth (SBW) relates to the number of metabolites we can observe without spectral aliasing. For example, in hyperpolarized [1-^{13}C]pyruvate studies at 3T, 500 Hz SBW is a reasonable range to observe the pyruvate and its products, [1-^{13}C]lactate and [1-^{13}C]alanine. Here we fixed spectral resolution = 10 Hz and FOV = 16 × 16 cm^2. SBW is determined by ΔT, which is the retracing period (in Equation 4) to the same k-space position.

$$SBW = \frac{1}{\Delta T} \quad (4)$$

Experimental Comparison

All the phantom and in vivo studies were conducted on a 3.0 T GE clinical scanner (GE Healthcare, Waukesha, WI, USA.) with maximum gradient amplitude of 40 mT/m and maximum slew rate of 150 mT/m/ms. All the animal studies conducted were approved by the Institutional Animal Care and Use Committee (IACUC).

Sequence Design Parameters for Concentric Rings Trajectory—CRT was implemented into the readout window of a 2D gradient echo (GRE) slice-selective pulse sequence. The spectroscopic imaging module consisted of readout window duration T_{readout} = 100 ms, corresponding to a nominal spectral resolution of Δf = 10 Hz, and a SBW = 500

Hz, which set the duration of each revolution to ΔT = 2 ms. The achievable in-plane isotropic spatial resolution was 3.67 mm, which was limited by the slew rate and by the SBW. For the ^{13}C phantom study, the flip angle (FA) was set to be constant for each excitation. In the hyperpolarized studies, a progressive flip angle technique [34] was applied in order to equalize the signal across excitations. Temporal interleaves were implemented by appropriate delay of the readout trajectory in order to increase spectral bandwidth.

^{13}C Phantom Spectroscopic Imaging Comparison—In order to evaluate the feasibility of CRT, we carried out comparison studies between CRT, spiral, and EPSI trajectories based on the similar prescriptions. A 4-compartment phantom for Carbon-13 was used, which included 1.0 M ^{13}C bicarbonate, 2.0 M ^{13}C formate, 1.0 M [1-^{13}C]lactate, and 1.0 M [1-^{13}C]alanine. For localization, T2-weighted ^{1}H anatomic MR images were acquired in sagittal, axial, and coronal views. CRT sequence was used with the basic prescriptions: FOV= 8×8 cm^2, resolution = 3.67×3.67 mm^2, TE/TR = 3.4 ms/ 5 s, SBW = 500 Hz, FA = 90 °, readout window $T_{readout}$ = 100 ms, and 11 rings were encoded. TR = 5 s was used for the full T1 relaxation of the ^{13}C components in the phantom. Since metabolites resonance range was about 700 Hz at 3.0 T, we did temporal interleaving to double the SBW from 500 Hz into 1000 Hz. The total scan time was 1min 50 s = 5 s (TR) × 11 (number of phase encoding rings) × 2 (interleaves).

We designed a symmetric EPSI trajectory (Nyquist-constrained) counterpart and time-optimal a spiral spectroscopic trajectory counterpart, which were implemented in the same pulse sequence scheme with CRT. Owing to the same prescriptions of 3.67 mm resolution and SBW = 500Hz, the symmetric EPSI trajectory was designed to have 50 odd echoes and 50 even echoes, including ramp sampling. It need twice the number of excitations as the CRT to cover the same FOV. As for spiral spectroscopic trajectory with respect of the design of of 8×8 cm^2 FOV and 3.67 mm isotropic resolution prescription, it only had 7 echoes in each TR, given the readout window duration, thus this single-shot spiral had the SBW = 68.6 Hz. In order to have comparable SBW with CRT and EPSI, spiral trajectory required multiple temporal interleaves.

The same 4-compartment phantom for Carbon-13 was used in the comparison studies. TE/TR = 3 ms/ 5 s was used for all the trajectories. The symmetric EPSI trajectory required 22 excitations and one temporal interleave to have comparable 1000 Hz SBW. For each readout, the data was separated into 50 odd echoes and 50 even echoes, and then reconstructed by 3D gridding to be two 22×22×50 matrices. The spiral trajectory required additional 14 interleaves to have 1000 Hz SBW. The raw data was 3D gridded into a 22×22×50 matrix. The total scan time was 1 min 50 s = 5 s (TR) × 11 (number of phase encoding rings) × 2 (interleaves) for CRT, 3 min 40 s = 5 s (TR) × 22 (number of phase encoding rings) × 2 (interleaves) for EPSI and 1 min 15 s = 5 s (TR) × 15 (interleaves) for spiral.

Hyperpolarized ^{13}C in vivo Spectroscopic Imaging—In vivo experiments were performed on normal Sprague-Dawley strain rats, with weight about 500 g. For all the rats, a tail vein catheter was placed immediately before the hyperpolarized MR study. Next, the isoflurane anesthetized rats were placed on a water-filled, temperature-controlled pad that

was heated to approximately 37 C° and positioned inside of the coil. We monitored the respiration and heart rate of the rats during the experiments.

Initially, T2-weighted ^{1}H anatomic MR images were acquired in sagittal, axial, and coronal views. The subsequent hyperpolarized ^{13}C scans were prescribed on the chosen slices. A mixture of [1-^{13}C] pyruvic acid and the trityl radical (tris methyl sodium salt; GE Healthcare) was polarized using the HyperSense polarizer (Oxford Instruments, Oxford, UK.). After the mixture was polarized, it was rapidly dissolved into a pH-balanced Tris buffer solution, targeting a hyperpolarized 100 mmol/L pyruvate solution with a neutral pH. Next, the solution was quickly transported to the MR scanner and 2.2 mL was injected into the rat over 12 s. The imaging data acquisition was initiated 30 s after the start of the pyruvate injection to coincide with the peak lactate signal. A slice-selective pulse sequence with a progressive flip angle excitation pulse using CRT was performed using a TE/TR = 3.4/200 ms, readout window $T_{readout}$ = 100 ms, and 11 rings. Additional sequence prescriptions for rat studies included: FOV= 8×8 cm^2, slice thickness of 10 mm, resolution = 3.67×3.67 mm^2, and 500 Hz SBW. The total scan time was 2.2 s. For this study, the total scan time could be reduced by 35% by decreasing TR. We carried out an in vivo comparison study between CRT and symmetric EPSI, TE/TR = 3.4/250 ms was used for CRT while for the symmetric EPSI comparison, TE/TR = 3.4/200 ms was used.

Parallel Imaging with Concentric Rings

Parallel imaging is favorable for hyperpolarized ^{13}C imaging because the shorter scan time reduces SNR losses due to T1 decay and metabolism during the acquisition, especially in larger, humansized FOV 2D MRSI or 3D MRSI applications that require large numbers of encoding steps. In non-hyperpolarized imaging, undersampling of k-space in parallel imaging reduces the acquisition time but at the trade-off of losing SNR, as Equation 5 shows: [36]

$$SNR_{und}=\frac{SNR_{full}}{g\sqrt{R}}. \quad (5)$$

SNR_{und} and SNR_{full} are the undersampled and fully sampled SNR respectively, and R is the acceleration factor. The g-factor, g, is spatially variant noise enhancement that depends on the receiver coil array and sampling pattern.

However, the inherent signal of hyperpolarized ^{13}C imaging is limited. With undersampling, the given amount of total magnetization can be distributed into fewer excitations where each excitation has more signal. In fact, reduced acquisition time may translate into higher image SNR due to the reduced T1 relaxation [15]. As a result, parallel imaging does not result in losing inherent signal if a progressive flip angle [34] is applied (shown in Equation 6). This results in an undersampled SNR as

$$SNR_{und}=\frac{SNR_{full}}{g}. \quad (6)$$

Simulation of G-factor—Given the same phase-array coil sensitivity, the g-factor is determined by the sampling pattern. A Monte-Carlo technique, which is also known as pseudo replica method [37], was used to calculate g-factor maps of a simulated 8-channel phased-array coil and 4-fold undersampling with CRT and rectilinear Cartesian (*i.e.*, EPSI) trajectories. Fully encoded series of images with identical parameters were simulated. Out of this image series, an SNR_{full} map of the fully encoded image can be derived by taking the mean and the standard deviation on a pixel-by-pixel basis throughout the image series. Undersampling was achieved by uniformly skipping phase encodings for both CRT and Cartesian counterparts. Similarly, after reconstruction an SNR_{und} map of undersampled encoded image was generated and a g-factor map was computed by the Equation 5.

The simulated g-factor maps were 256× 256 and cropped to display circular FOV. CRT's g-factor maps were generated by using fully sampled 128 rings and undersampled 32 rings respectively, while the Cartesian (EPSI) g-factor map was generated by fully sampled 256 phase encodings and undersampled 64 phase encodings. We used conjugate gradient SENSE (CG-SENSE) [38] without regularization for the reconstruction. The number of pseudo replicas was 50 for both sampling patterns.

Parallel Imaging for Hyperpolarized ^{13}C in vivo Spectroscopic Imaging—To evaluate the feasibility of parallel imaging using CRT, a hyperpolarized in vivo experiment was performed on normal Sprague-Dawley strain rats. An 8-channel ^{13}C phased-array rat coil was constructed especially for the study with the coils distributed isotropically around the animal in the axial plane. We redesigned the CRT sequence to have a 420 Hz SBW as a tradeoff for finer spatial resolution, and 10 Hz nominal spectral resolution. A slice-selective pulse sequence with a progressive flip angle excitation pulse using CRT was performed using a TE/TR = 3.4/320 ms. Additional sequence prescriptions for this rat study included: FOV= 8×8 cm^2, slice thickness of 20 mm, resolution = 2.5×2.5 mm^2 (using a maximum gradient amplitude of 50 mT/m and maximum slew rate of 200 mT/m/ms). We prospectively undersampled CRT by 1.45 spatially, using 11 rings instead of the 16 rings required for full sampling. The inner 6 rings were fully sampled for calibration and outer 5 rings were evenly undersampled by 2. The reconstructed results were 32×32×42 (spatial + spatial + spectral) matrices.

Reconstruction and Data Processing

Image reconstruction and postprocessing were carried out in Matlab. We applied density compensation to the non-Cartesian raw data, 3D gridded it into Cartesian data, and then performed an FFT. Gridding and FFT were done by using Fessler's non-uniform fast Fourier transform (NUFFT) toolbox [39] with min-max Kaiser-Bessel kernel interpolation and twice oversampling. The matrix size of the reconstructed CRT image was $2N_{ring} \times 2N_{ring} \times N_{rev}$ after 3D gridding (2D spatial + 1D spectral). The same NUFFT reconstruction method was also applicable for symmetric EPSI (Nyquist-constrained), flyabck EPSI and spiral spectroscopic imaging. In our symmetric EPSI reconstruction, for each readout, the data was separated into 50 odd echoes and 50 even echoes, and then reconstructed by 3D gridding respectively, and finally average the two results.

For spectroscopic imaging data, peak heights were assessed to quantify SNR. The noise was calculated, using an area outside of the object but within the FOV, as standard deviation of the whole spectra. The same area (relatively uniform) were chosen to analyze SNR of CRT, spiral and EPSI. Median signal values among all the voxels in the selected area, along with standard deviation were used to quantify the SNR of each metabolites. Metabolites SNR were also normalized to the acquisition time to analyze SNR efficiency.

For parallel imaging simulations, non-regularized iterative SENSE [38] reconstruction and Monte-Carlo method were performed to compute the g-factor maps. For parallel imaging in vivo experiments, sensitivity maps were obtained by the auto-calibration method EPSIRiT [40] and L1-regularized SENSE was used for reconstruction.

Results

Theoretical Comparison of the Concentric Rings Trajectory with EPSI and Spiral

In the following, we compared CRT with EPSI and spiral MRSI trajectories in terms of resolution, acquisition time, SNR efficiency, and spectral bandwidth.

Acquisition Time—As shown in Figure 3 (top-left), since both symmetric EPSI and flyback EPSI have the same number of phase encodings and interleaves are not required, they result in the same total acquisition time for each individual resolution. Compared with EPSI, CRT requires fewer phase encodings and no interleaves, so it results in saving half of the total acquisition time given the same TR. For the spiral trajectory design, we used a time-optimal spiral in order to optimize the gradient duration and required interleaving of the spiral trajectory to fulfill the spectral bandwidth requirement (500 Hz). Spirals are the most time efficient of all the trajectories, while CRTs are twice as fast as EPSI trajectories.

SNR Efficiency—Figure 3 (top-right) shows the SNR efficiency of different trajectories with various resolution prescriptions. The SNR loss for flyback EPSI is mostly due to its low duty cycle. The finer the resolution is, the lower the duty cycle will be and SNR efficiency decreases as the flyback portion requires more time. Although the duty cycle for symmetric EPSI is 100% (including ramp sampling), the non-uniform k-space sampling resulting from the ramp part of the trapezoid waveform reduces the SNR efficiency to some extent. The SNR efficiency is very high for symmetric EPSI but not 100%. As the resolution gets coarser, the ramp portion is smaller, so the SNR efficiency is higher. For the constant slew rate spiral trajectories, the SNR efficiency decreases as the resolution becomes coarser with a fixed FOV since there is proportionally less outer k-space sampling where spirals are more uniform than inner k-space. Non-uniformity results in the most of the SNR loss of spirals while duty cycle results in a smaller fraction of the loss. Benefiting from the design of constant slew rate, the spiral trajectories provide even better SNR efficiency than flyback EPSI and CRT. CRT offers a constant SNR efficiency of $\frac{\sqrt{3}}{2}$, which is better than flyback EPSI with the chosen prescriptions. The loss of SNR efficiency for CRT is caused by the non-uniformity.

Spectral Bandwidth—EPSI traverses a rectilinear line in k-space for each retracing period, CRT traverses a circle, while spiral traverses the whole spatial k-space in each period. Given the same traversing velocity (determined by the gradient waveforms), accordingly, the achieved SBW for EPSI, CRT, and spirals are decreasing in order, as shown in Figure 3 (bottom-left) without interleaves. To exploit the maximum spectral bandwidth, both symmetric EPSI and flyback EPSI result in the same waveform design thus achieving the same spectral bandwidth. They are only slightly better than CRT since flyback EPSI requires flyback time and symmetric EPSI (Nyquist-constrained) does not critically exploit the whole spectral bandwidth.

However, CRT and spiral trajectories are more scan-time-efficient compared with EPSI. If we take advantage of scan-time-efficiency by applying interleaves in temporal domain, we can increase SBW. In Figure 3 (bottom-right), the SBW of all trajectories was computed by accounting for the interleaves in time domain constrained for the same total acquisition time. Considering this tradeoff, spiral trajectories offer the best SBW, while CRT's spectral bandwidth is doubled compared to EPSI. The non-monotonicity of the spiral trajectories SBW with respect to resolution in this analysis is due to using an integer number of interleaves.

^{13}C Phantom Spectroscopic Imaging Using CRT

As we could tell from the 4-compartment phantom for Carbon-13 (Figure 4), the singlet peaks of ^{13}C bicarbonate(on the top left), [1-^{13}C]lactate (on the top right) and [1-^{13}C]alanine (on the bottom left) and doublet of ^{13}C formate (on the bottom right) were well resolved when using interleaved CRT with SBW = 1000 Hz. The ^{13}C 2D image was obtained by spatially zero padding and projecting along the spectral domain, in order to display all the compartments. At this resolution, we observed that the edges of the different compartments were well resolved in ^{13}C 2D image and it matched well with the proton reference image.

Comparison of CRT, Spiral and EPSI on ^{13}C Phantom

Figure 5 shows the phantom comparison results from CRT, spiral and EPSI (from left to right). The first row in Figure 5 shows 2D images obtained by twice spatially zero padding and projecting along the spectral domain. While all MRSI trajectories showed very comparable image quality, we did observe a slight blurring with the spiral and EPSI trajectories (yellow arrows) compared to the CRT. For the spiral trajectory, we observed an isotropic approximately half-voxel blurring, while for EPSI we observed approximately half-voxel blurring in the readout direction (left/right). These might be the result of induced eddy currents, which could measured and corrected for by performing trajectory measurements.

For SNR comparison, we selected 9 voxels (in red boxes) in the ^{13}C bicarbonate chamber. For comparison, these raw SNR values were normalized by the acquisition time, as shown in Table 1. Spiral MRSI had a superior normalized SNR over CRT and EPSI, which coincides with the comparison plot shown in Figure 3. Overall, CRT provided some improvement in image quality (without using any trajectory measurements) but a reduced SNR efficiency.

Hyperpolarized ^{13}C In Vivo Spectroscopic Imaging with Concentric Rings

The imaging plane was chosen at the abdomen of a rat in axial view (fin Figure 6). The kidneys of rats showed the high uptake of pyruvate and its conversion to alanine and lactate. Spatially, the [1-^{13}C] pyruvate image (Fig. 6b) and [1-^{13}C] lactate image (Fig. 6c) captured the structure of the kidneys and vasculature, and metabolic conversion. Resolution of different metabolites was captured in the ^{13}C spectrum with 500 Hz SBW (a selected voxel is shown in Fig. 6d). Pyruvate and lactate images were twice zero padded to have a displayed resolution of 1.83×1.83 mm^2. The total scan time was 2.2 s.

Comparison between Concentric Rings and EPSI with Hyperpolarized ^{13}C In Vivo

We compared CRT and a Nyquist-constrained EPSI counterpart with the same prescriptions, where the total scan time for CRT was 2.75 s while it was 4.4 s for EPSI. In Figure 7, 2D images were obtained from the projection along the spectral domain. Both methods captured the anatomical structure and metabolic conversion with comparable quality. As the red arrows show, the through-plane flow in the major vessels resulted in ghosting replicas in the phase encoding direction for EPSI. However, pulsatile flow in CRT will manifest as low-amplitude background halos [26], which may have lead to increased background signal in CRT.

Parallel Imaging with the Concentric Rings

Simulated G-factor—As the simulated g-factor maps (in Figure 8) confirm, the non-rectilinear circular sampling pattern of CRT results in more incoherent noise amplification than Cartesian counterparts such as EPSI. Noise is amplified by 3–4 times at discrete locations for the Cartesian undersampling pattern due to the worse conditioning of the reconstruction problem. For CRT, the noise was more uniformly distributed spatially, resulting in a noise amplification of no more than 2.5 for this simulated 8-channel array with 4× undersampling. (In conjunction with appropriate regularization, the g-factor can be further improved.) The non-Cartesian sampling pattern of concentric rings is advantageous because it makes the noise amplification incoherent thus lowering the g-factor of the whole space.

Parallel Imaging for Hyperpolarized ^{13}C in vivo Spectroscopic Imaging—The hyperpolarized ^{13}C-pyruvate in vivo spectroscopic imaging in Figure 9 demonstrates for the first time parallel imaging with CRT. The direct reconstruction of the prospectively undersampled data resulted in the circular aliasing artifacts (yellow arrows) in the spatial domain for each coil image (top row of Figure 9). These coil images were generated from the projection along the spectral domain for display. The total scan time was 3.52 s, achieved by prospective 1.45× acceleration. With a parallel imaging reconstruction, the undersampling aliasing was eliminated and good image quality was achieved, as is shown on the bottom left of Figure 9. The bottom right plot shows the spectrum of a selected kidney voxel, clearly showing pyruvate and its conversion to lactate.

Discussion

CRT provides a competitive alternative to existing ^{13}C spectroscopic imaging acquisition methods. Our CRT sequence requires half the number of excitations compared to EPSI. This has an advantage in two-fold acquisition time savings. In addition, the T1 decay is reduced, which leads to overall higher SNR [15]. The acquisition time saving can be traded off for an increased spectral bandwidth through interleaving. We also showed that even though CRT samples k-space non-uniformly, its SNR efficiency is still $\frac{\sqrt{3}}{2} \approx 0.87$ of uniform sampling.

We expect that the concentric rings trajectory will be more robust to system imperfections than spirals or critical symmetric EPSI. For all trajectories, any gradient timing delay or eddy currents will results in some artifacts. In spirals, these cause spatial blurring. In critical symmetric EPSI, one effect of these is odd-even echo inconsistency which results in spectral aliasing. This is analogous to ghosting artifacts in EPI [41]. For CRT, delays and first-order eddy currents result in benign image rotations [26]. More importantly, no spectral aliasing or spatial aliasing artifacts will be observed.

One of the advantages of using CRT is robustness to flow, that was also reported in [26]. Pulsatile flow is distributed in two dimensions by CRT and spiral [42]. In contrast, EPSI trajectories can suffer from significant pulsatile flow artifacts where flow results in replicas in phase encoding direction.

Combining CRT with parallel imaging for hyperpolaizated ^{13}C imaging is also very promising. Undersampling is achieved by acquiring fewer rings than what are necessary for in plane full-FOV. We showed in Monte Carlo simulations that with CRT the resulting g-factor due to undersampling is lower than for Cartesian undersampling. The reason is that CRT undersamples isotropically in-plane, whereas Cartesian imaging can accelerate only in the phase-encoding directions. As a result, CRT acquisitions can better utilize the multi-dimensional spatial variation of the coils sensitivities to improve the conditioning of the reconstruction. Furthermore, for hyperpolaizated ^{13}C we do not suffer from the usual $\sqrt{R}$ loss of SNR due to subsampling. The reason is that the total magnetization can be redistributed optimally to fewer number of excitations. Hyperpolarized ^{13}C parallel imaging with CRT is essential for the large FOV applications, *e.g.*, metastatic cancer imaging.

There are some possible extensions of CRT for ^{13}C MRSI: (1) the shorter scan time could be amortized for dynamic MRSI to track perfusion and metabolism kinetics; (2) 3D MRSI to cover a larger volume in vivo; (3) variable-density undersampling designs for parallel imaging, maintaining the inner k-space fully sampled to capture the intrinsic contrast and outer k-space undersampled for resolution and acceleration; (4) compressed sensing, taking advantages of intrinsically sparse ^{13} C spectra [18, 19]. These improvements could further reduce the total scan time.

We initially performed high resolution ^{1}H MRSI studies to evaluate the CRT sequence. Through these studies, we observed some spatial and spectral blurring, which we were able to model as gradient induced phase errors. We measured this to be approximately quadratically varying with total gradient magnitude and linearly time-accumulating. Based

on these measurements, we applied a quadratic phase compensation for ^{1}H MRSI data that resulted in effective removal of the blurring effects. We eliminated the possibilities of concomitant gradients [43] and first order eddy currents, but did not determine the source of these phase errors. The blurring was only prominent in high resolution ^{1}H MRSI data. For ^{13}C data, the amount of phase observed would not result in noticeable blurring, and we observed no visible artifacts. We also observed the phase error varied between different GE 3.0 T scanners, so we suspect it is related to some gradient system compensations.

Conclusion

Our preclinical studies have demonstrated the potential and feasibility of using concentric rings in hyperpolarized ^{13}C MRSI for a two-fold acceleration over EPSI, with inherent robustness to flow artifacts, gradient system delay and first order eddy currents. Parallel imaging will also benefit from this trajectory for hyperpolarized ^{13}C imaging. Compared with existing methods, the concentric rings trajectory provides flexible and robust trade-off between acquisition time and spectral bandwidth, thereby acting as an effective alternative for hyperpolarized ^{13}C MRSI.

Supplementary Material

Refer to Web version on PubMed Central for supplementary material.

Acknowledgement

The authors would like to thank Dr. Robert Bok for his assistance in animal studies, Peter Shin for his help to implement the EPSI waveforms, Dr. Ralph Hurd for his kindness of providing the ^{13}C phantom, and Dr. Anita Flynn for her considerable efforts to make the 8-channel phased-array rat coil. This work was supported by NIH grants R00-EB012064; P41-EB013598, a UCSF Department of Radiology and Biomedical Imaging Seed Grant, and the Sloan Research Fellowship.

References

1. Kurhanewicz J, Vigneron DB, Brindle K, Chekmenev EY, Comment A, Cunningham CH, DeBerardinis RJ, Green GG, Leach MO, Rajan SS, et al. Analysis of cancer metabolism by imaging hyperpolarized nuclei: prospects for translation to clinical research. Neoplasia (New York, NY). 2011; 13:81.
2. ArdenkjærLarsen JH, Fridlund B, Gram A, Hansson G, Hansson L, Lerche MH, Servin R, Thaning M, Golman K. Increase in signal-to-noise ratio of > 10,000 times in liquid-state nmr. Proceedings of the National Academy of Sciences. 2003; 100:10158–10163.
3. Nelson SJ, Kurhanewicz J, Vigneron DB, Larson PEZ, Harzstark AL, Ferrone M, van Criekinge M, Chang JW, Bok R, Park I, Reed G, Carvajal L, Small EJ, Munster P, Weinberg VK, ArdenkjaerLarsen JH, Chen AP, Hurd RE, Odegardstuen LI, Robb FJ, Tropp J, Murray JA. Metabolic imaging of patients with prostate cancer using hyperpolarized [1-13c]pyruvate. Science Translational Medicine. 2013; 5:198ra108.
4. Cunningham CH, Vigneron DB, Chen AP, Xu D, Nelson SJ, Hurd RE, Kelley DA, Pauly JM. Design of flyback echo-planar readout gradients for magnetic resonance spectroscopic imaging. Magnetic resonance in medicine. 2005; 54:1286–1289. [PubMed: 16187273]
5. Yen YF, Kohler S, Chen A, Tropp J, Bok R, Wolber J, Albers M, Gram K, Zierhut M, Park I, Zhang V, Hu S, Nelson S, Vigneron D, Kurhanewicz J, Dirven H, Hurd R. Imaging considerations for in vivo 13c metabolic mapping using hyperpolarized 13c-pyruvate. Magnetic Resonance in Medicine. 2009; 62:1–10. [PubMed: 19319902]

6. Ramirez MS, Lee J, Walker CM, Sandulache VC, Hennel F, Lai SY, Bankson JA. Radial spectroscopic mri of hyperpolarized [1-13c] pyruvate at 7 tesla. Magnetic Resonance in Medicine. 2014; 72:986–995. [PubMed: 24186845]
7. Mayer D, Levin YS, Hurd RE, Glover GH, Spielman DM. Fast metabolic imaging of systems with sparse spectra: application for hyperpolarized 13C imaging. Magn Reson Med. 2006; 56:932–937. [PubMed: 16941617]
8. Josan S, Hurd R, Park JM, Yen YF, Watkins R, Pfefferbaum A, Spielman D, Mayer D. Dynamic metabolic imaging of hyperpolarized [2–13c]pyruvate using spiral chemical shift imaging with alternating spectral band excitation. Magnetic Resonance in Medicine. 2014; 71:2051–2058. [PubMed: 23878057]
9. Leupold J, Månsson S, Petersson JS, Hennig J, Wieben O. Fast multiecho balanced ssfp metabolite mapping of (1)h and hyperpolarized (13)c compounds. MAGMA. 2009; 22:251–256. [PubMed: 19367422]
10. Wiesinger F, Weidl E, Menzel MI, Janich MA, Khegai O, Glaser SJ, Haase A, Schwaiger M, Schulte RF. Ideal spiral csi for dynamic metabolic mr imaging of hyperpolarized [1-13c]pyruvate. Magn Reson Med. 2012; 68:8–16. [PubMed: 22127962]
11. Gordon JW, Niles DJ, Fain SB, Johnson KM. Joint spatial-spectral reconstruction and k-t spirals for accelerated 2d spatial/1d spectral imaging of 13c dynamics. Magnetic Resonance in Medicine. 2014; 71:1435–1445. [PubMed: 23716402]
12. von Morze C, Reed G, Shin P, Larson PEZ, Hu S, Bok R, Vigneron DB. Multi-band frequency encoding method for metabolic imaging with hyperpolarized [1-(13)c]pyruvate. J Magn Reson. 2011; 211:109–113. [PubMed: 21596601]
13. Lau AZ, Chen AP, Ghugre NR, Ramanan V, Lam WW, Connelly KA, Wright GA, Cunningham CH. Rapid multislice imaging of hyperpolarized 13c pyruvate and bicarbonate in the heart. Magn Reson Med. 2010; 64:1323–1331. [PubMed: 20574989]
14. Cunningham CH, Chen AP, Lustig M, Hargreaves BA, Lupo J, Xu D, Kurhanewicz J, Hurd RE, Pauly JM, Nelson SJ, Vigneron DB. Pulse sequence for dynamic volumetric imaging of hyperpolarized metabolic products. J Magn Reson. 2008; 193:139–146. [PubMed: 18424203]
15. Arunachalam A, Whitt D, Fish K, Giaquinto R, Piel J, Watkins R, Hancu I. Accelerated spectroscopic imaging of hyperpolarized c-13 pyruvate using sense parallel imaging. NMR in Biomedicine. 2009; 22:867–873. [PubMed: 19489035]
16. Tropp J, Lupo JM, Chen AP, Calderon P, McCune D, Grafendorfer T, OzturkIsik E, Larson PE, Hu S, Yen YF, Robb F, Bok R, Schulte R, Xu D, Hurd R, Vigneron D, Nelson S. Multi-channel metabolic imaging, with sense reconstruction, of hyperpolarized [1-13c] pyruvate in a live rat at 3.0 tesla on a clinical mr scanner. J Magn Reson. 2011; 208:171–177. [PubMed: 21130012]
17. Ohliger MA, Larson PEZ, Bok RA, Shin P, Hu S, Tropp J, Robb F, Carvajal L, Nelson SJ, Kurhanewicz J, Vigneron DB. Combined parallel and partial fourier mr reconstruction for accelerated 8-channel hyperpolarized carbon-13 in vivo magnetic resonance spectroscopic imaging (mrsi). J Magn Reson Imaging. 2013; 38:701–713. [PubMed: 23293097]
18. Larson PEZ, Hu S, Lustig M, Kerr AB, Nelson SJ, Kurhanewicz J, Pauly JM, Vigneron DB. Fast dynamic 3d mr spectroscopic imaging with compressed sensing and multiband excitation pulses for hyperpolarized 13c studies. Magn Reson Med. 2011; 65:610–619. [PubMed: 20939089]
19. Hu S, Lustig M, Balakrishnan A, Larson PEZ, Bok R, Kurhanewicz J, Nelson SJ, Goga A, Pauly JM, Vigneron DB. 3d compressed sensing for highly accelerated hyperpolarized 13c mrsi with in vivo applications to transgenic mouse models of cancer. Magnetic Resonance in Medicine. 2010; 63:312–321. [PubMed: 20017160]
20. Weiss K, Sigfridsson A, Wissmann L, Busch J, Batel M, Krajewski M, Ernst M, Kozerke S. Accelerating hyperpolarized metabolic imaging of the heart by exploiting spatiotemporal correlations. NMR in Biomedicine. 2013; 26:1380–1386. [PubMed: 23616307]
21. Wilson DM, Keshari KR, Larson PEZ, Chen AP, Criekinge MV, Bok R, Nelson SJ, Macdonald JM, Vigneron DB, Kurhanewicz J. Multi-compound polarization by dnp allows simultaneous assessment of multiple enzymatic activities in vivo. J Magn Reson. 2010; 205:141–147. [PubMed: 20478721]

22. Chen AP, Hurd RE, Schroeder MA, Lau AZ, Gu Yp, Lam WW, Barry J, Tropp J, Cunningham CH. Simultaneous investigation of cardiac pyruvate dehydrogenase flux, krebs cycle metabolism and ph, using hyperpolarized [1,2-13c2]pyruvate in vivo. NMR Biomed. 2012; 25:305–311. [PubMed: 21774012]
23. Mansfield P. Spatial mapping of the chemical shift in nmr. Magn Reson Med. 1984; 1:370–386. [PubMed: 6571566]
24. Adalsteinsson E, Irarrazabal P, Topp S, Meyer C, Macovski A, Spielman DM. Volumetric spectroscopic imaging with spiral-based k-space trajectories. Magnetic resonance in medicine. 1998; 39:889–898. [PubMed: 9621912]
25. Kim DH, Spielman DM. Reducing gradient imperfections for spiral magnetic resonance spectroscopic imaging. Magnetic Resonance in Medicine. 2006; 56:198–203. [PubMed: 16724300]
26. Wu HH, Lee JH, Nishimura DG. Mri using a concentric rings trajectory. Magnetic Resonance in Medicine. 2008; 59:102–112. [PubMed: 17969074]
27. Wu, HH. PhD thesis. Stanford University; 2009 Sep. MAGNETIC RESONANCE IMAGING USING A CONCENTRIC RINGS K-SPACE TRAJECTORY.
28. Kwon KT, Wu HH, Shin T, Çukur T, Lustig M, Nishimura DG. Three-dimensional magnetization-prepared imaging using a concentric cylinders trajectory. Magnetic Resonance in Medicine. 2014; 71:1700–1710. [PubMed: 23818212]
29. Furuyama JK, Wilson NE, Thomas MA. Spectroscopic imaging using concentrically circular echo-planar trajectories in vivo. Magnetic Resonance in Medicine. 2012; 67:1515–1522. [PubMed: 22006586]
30. Hargreaves BA, Nishimura DG, Conolly SM. Time-optimal multidimensional gradient waveform design for rapid imaging. Magnetic resonance in medicine. 2004; 51:81–92. [PubMed: 14705048]
31. CVXResearch I. CVX: Matlab software for disciplined convex programming, version 2.0. 2012 Aug. http://cvxr.com/cvx.
32. Papoulis A. Generalized sampling expansion. Circuits and Systems, IEEE Transactions on. 1977; 24:652–654.
33. GregoryMetzger XH. Application of interlaced fourier transform to echo-planar spectroscopic imaging. J Magn Reson. 1997; 125:166–170. [PubMed: 9245375]
34. Zhao L, Mulkern R, Tseng CH, Williamson D, Patz S, Kraft R, Walsworth RL, Jolesz FA, Albert MS. Gradient-echo imaging considerations for hyperpolarized ^{129}xe mr. Journal of Magnetic Resonance, Series B. 1996; 113:179–183.
35. Tsai CM, Nishimura DG. Reduced aliasing artifacts using variable-density k-space sampling trajectories. Magnetic resonance in medicine. 2000; 43:452–458. [PubMed: 10725889]
36. Pruessmann KP, Weiger M, Scheidegger MB, Boesiger P. Sense: Sensitivity encoding for fast mri. Magnetic Resonance in Medicine. 1999; 42:952–962. [PubMed: 10542355]
37. Breuer FA, Kannengiesser SA, Blaimer M, Seiberlich N, Jakob PM, Griswold MA. General formulation for quantitative g-factor calculation in grappa reconstructions. Magnetic Resonance in Medicine. 2009; 62:739–746. [PubMed: 19585608]
38. Pruessmann KP, Weiger M, Börnert P, Boesiger P. Advances in sensitivity encoding with arbitrary k-space trajectories. Magnetic Resonance in Medicine. 2001; 46:638–651. [PubMed: 11590639]
39. Fessler JA, Sutton BP. Nonuniform fast fourier transforms using min-max interpolation. Signal Processing, IEEE Transactions on. 2003; 51:560–574.
40. Uecker M, Lai P, Murphy MJ, Virtue P, Elad M, Pauly JM, Vasanawala SS, Lustig M. Espirit— an eigenvalue approach to autocalibrating parallel mri: Where sense meets grappa. Magnetic Resonance in Medicine. 2014; 71:990–1001. [PubMed: 23649942]
41. Bernstein, MA.; King, KF.; Zhou, XJ. Handbook of MRI Pulse Sequence. USA: Elsevier Academic Press MA; 2004.
42. Pipe JG, Ahunbay E, Menon P. Effects of interleaf order for spiral mri of dynamic processes. Magnetic resonance in medicine. 1999; 41:417–422. [PubMed: 10080293]
43. Bernstein MA, Zhou XJ, Polzin JA, King KF, Ganin A, Pelc NJ, Glover GH. Concomitant gradient terms in phase contrast mr: Analysis and correction. Magnetic Resonance in Medicine. 1998; 39:300–308. [PubMed: 9469714]

44. Moriguchi H, Duerk JL. Bunched phase encoding (bpe): A new fast data acquisition method in mri. Magnetic Resonance in Medicine. 2006; 55:633–648. [PubMed: 16470597]

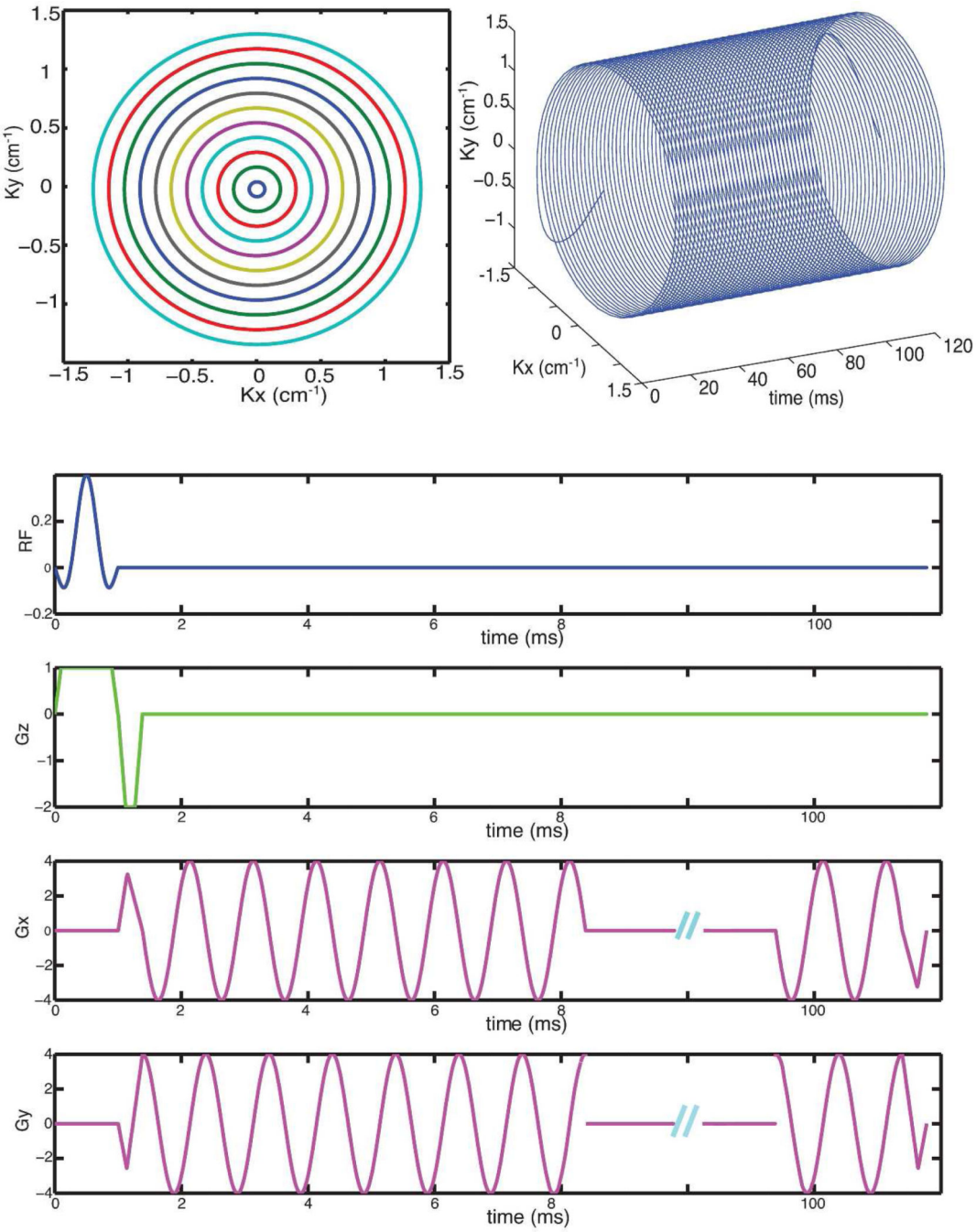

Figure 1.

Concentric rings trajectory and sequence design: top-left shows the spatial concentric rings k-space trajectory; top-right shows the spatial-spectral k-space trajectory; bottom shows the concentric rings GRE sequence for axial images.

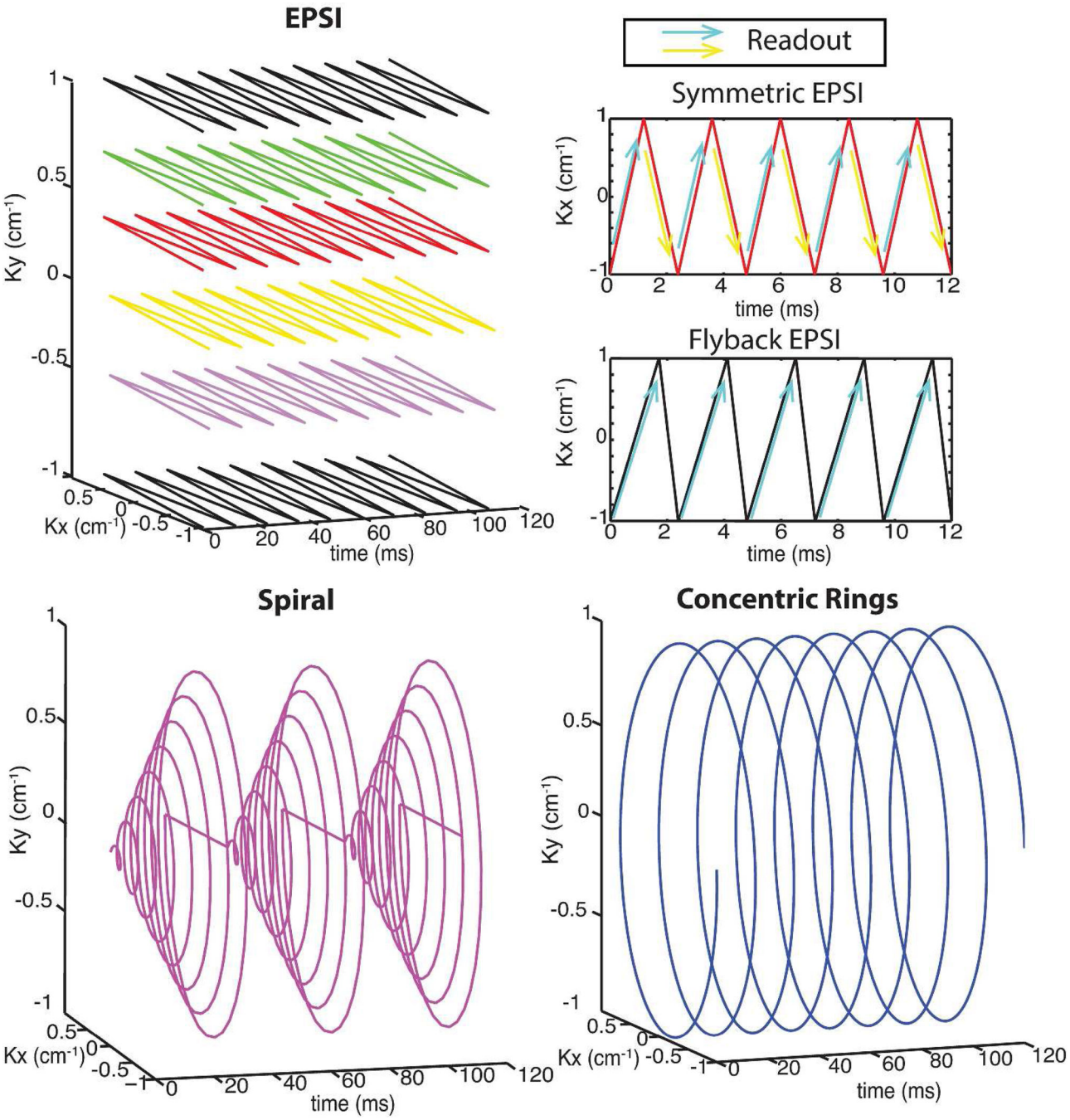

Figure 2.

K-space trajectories of EPSI, spiral and concentric rings spectroscopic imaging: the arrows illustrates the readout directions for both symmetric EPSI and flyback EPSI; for symmetric EPSI, we use different-colored arrows to differentiate the odd/even echoes for reconstruction.

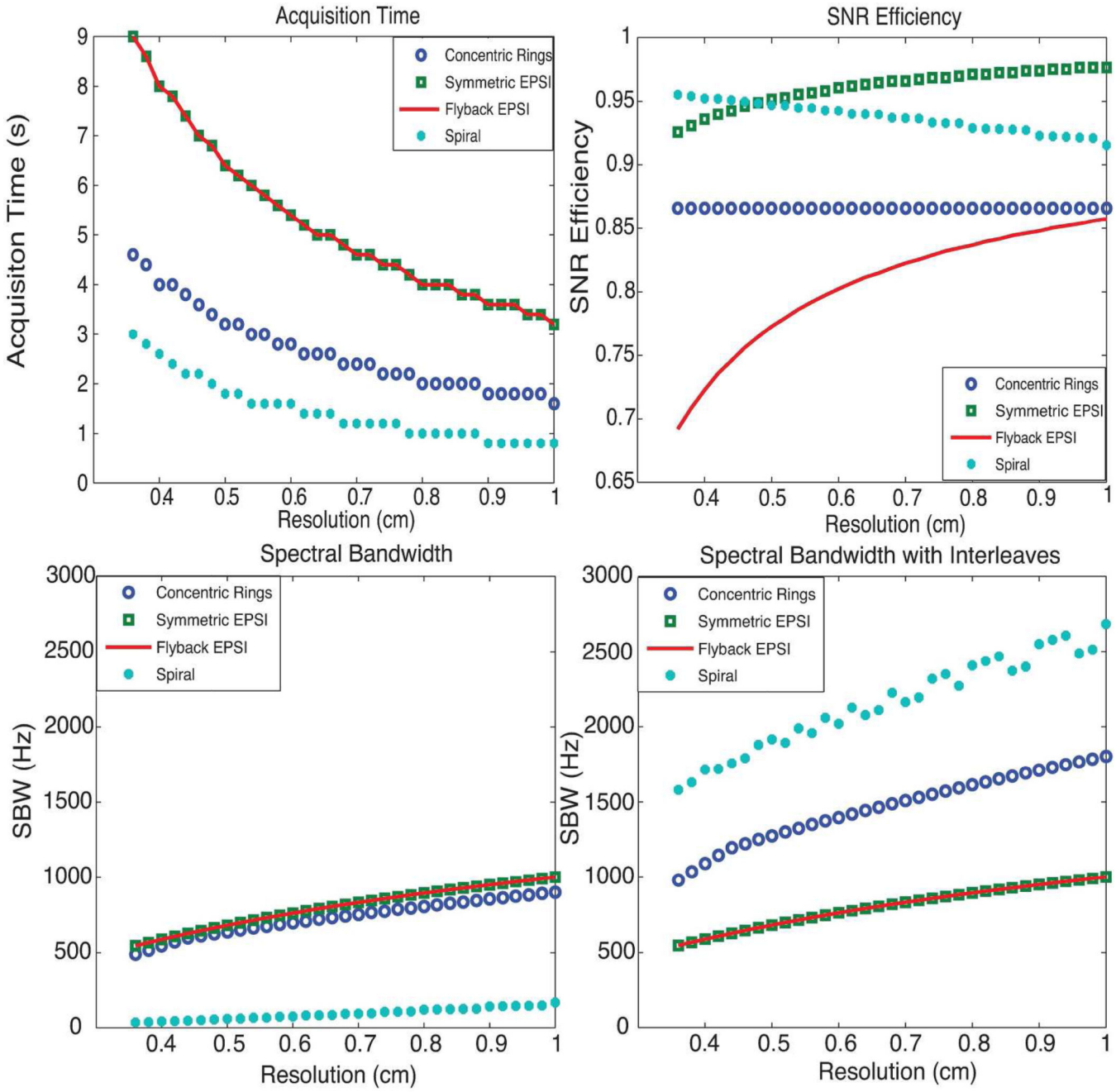

Figure 3.

Comparison of concentric rings, EPSI and spiral spectroscopic imaging: top-left shows the acquisition time; top-right shows the SNR efficiency; bottom-left and bottom-right show the SBW and SBW with spectral interleaves. CRT requires half of the total acquisition time compared with EPSI trajectories, offers about 87% SNR efficiency, and provides much wider spectral bandwidth than flyback EPSI and symmetric EPSI. Although nominally spirals are the most efficient trajectories, offering the best acquisition time and spectral bandwidth benefit while sacrificing the least SNR, they are limited by susceptibility to gradient infidelities.

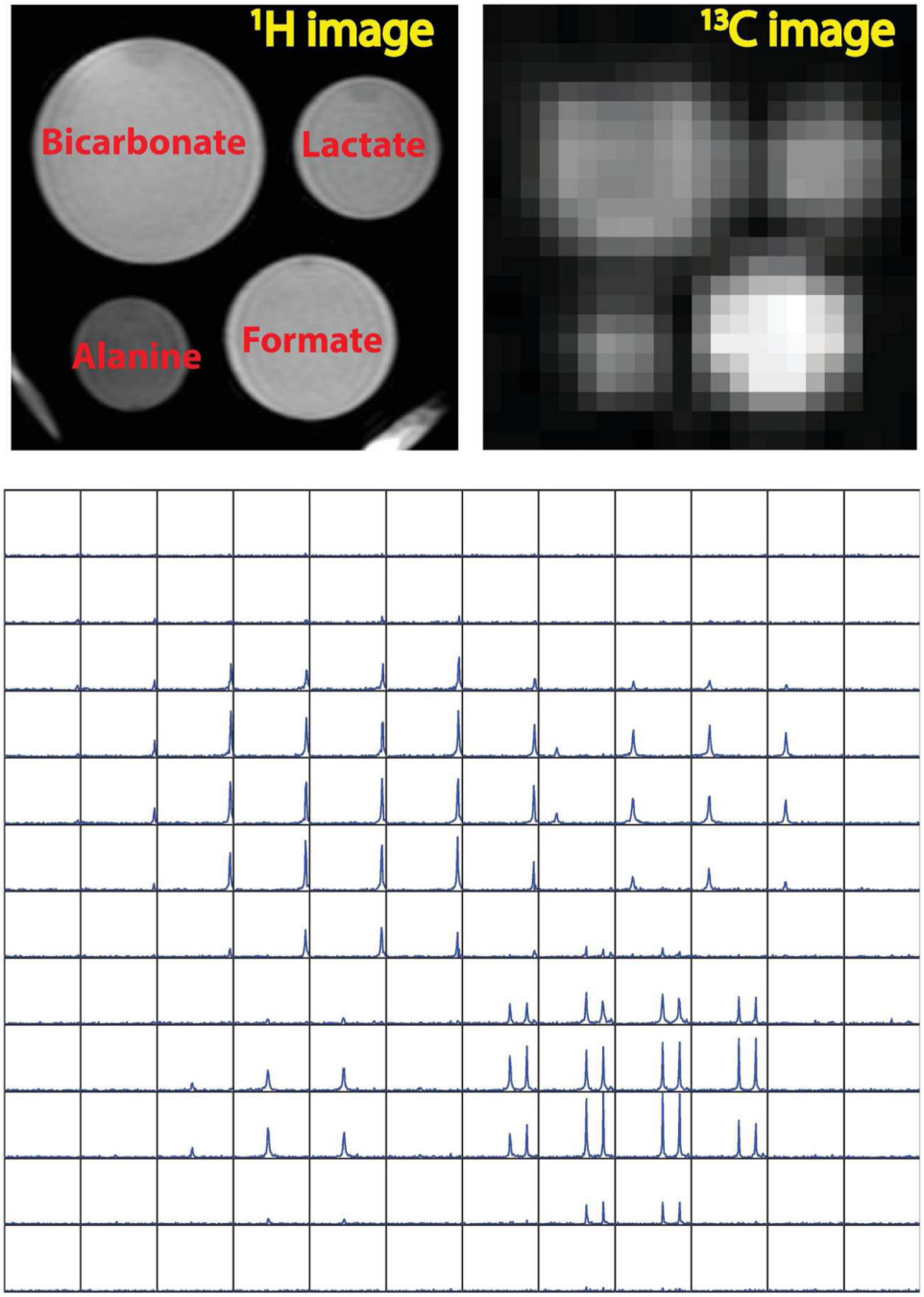

Figure 4.

^{13}C phantom study using CRT: (top-left) ^{1}H image localizer; (top-right) ^{13}C 2D image via projection on spectral domain; (bottom) spatial-spectral display for spectroscopic imaging. The displayed ^{13}C 2D image has the nominal spatial resolution of 1.83×1.83 mm^2 after zero padding. The reconstructed spatial-spectral (2D spatial+1D spectral) data matrix (22×22×100) was cropped to 12×12×100, and the SBW for each voxel was 1000 Hz. This was a non-hyperpolarized study, with the TR = 5 s and total acquisition time of 1min 50 s.

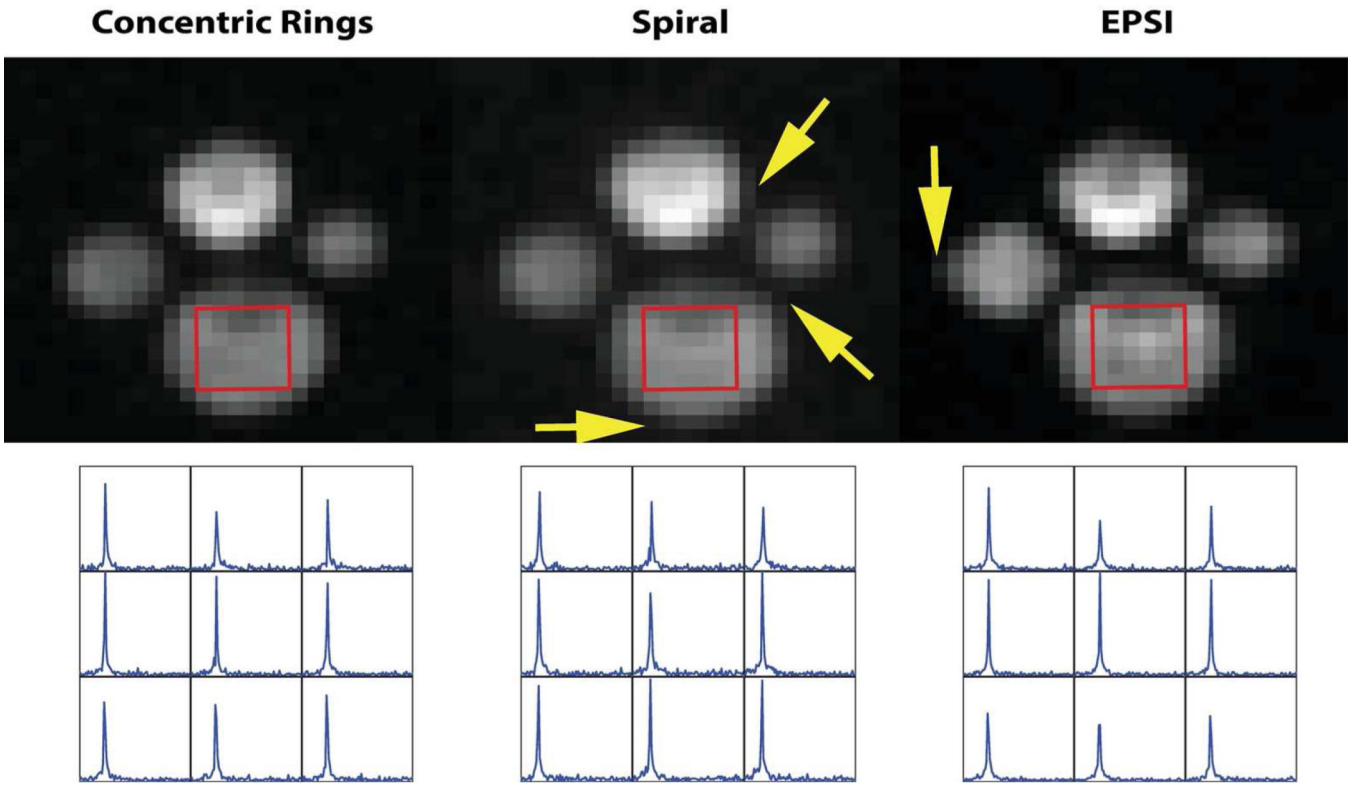

Figure 5.

Comparison of ^{13}C phantom spectroscopic imaging using CRT, Spiral and EPSI: the top row (from left to right) images were obtained from CRT, Spiral and EPSI respectively. They were created from spectroscopic images via projection along the spectral domain. The displayed ^{13}C 2D image has a nominal spatial resolution of 1.83×1.83 mm^2 after zero padding and was cropped into a 5×5 cm^2 ROI. The arrows show the slight blurring of spiral and EPSI. The bottom row (from left to right) plots are of ^{13}C bicarbonate spectra obtained from CRT, Spiral and EPSI, respectively, from the same 9 voxels.

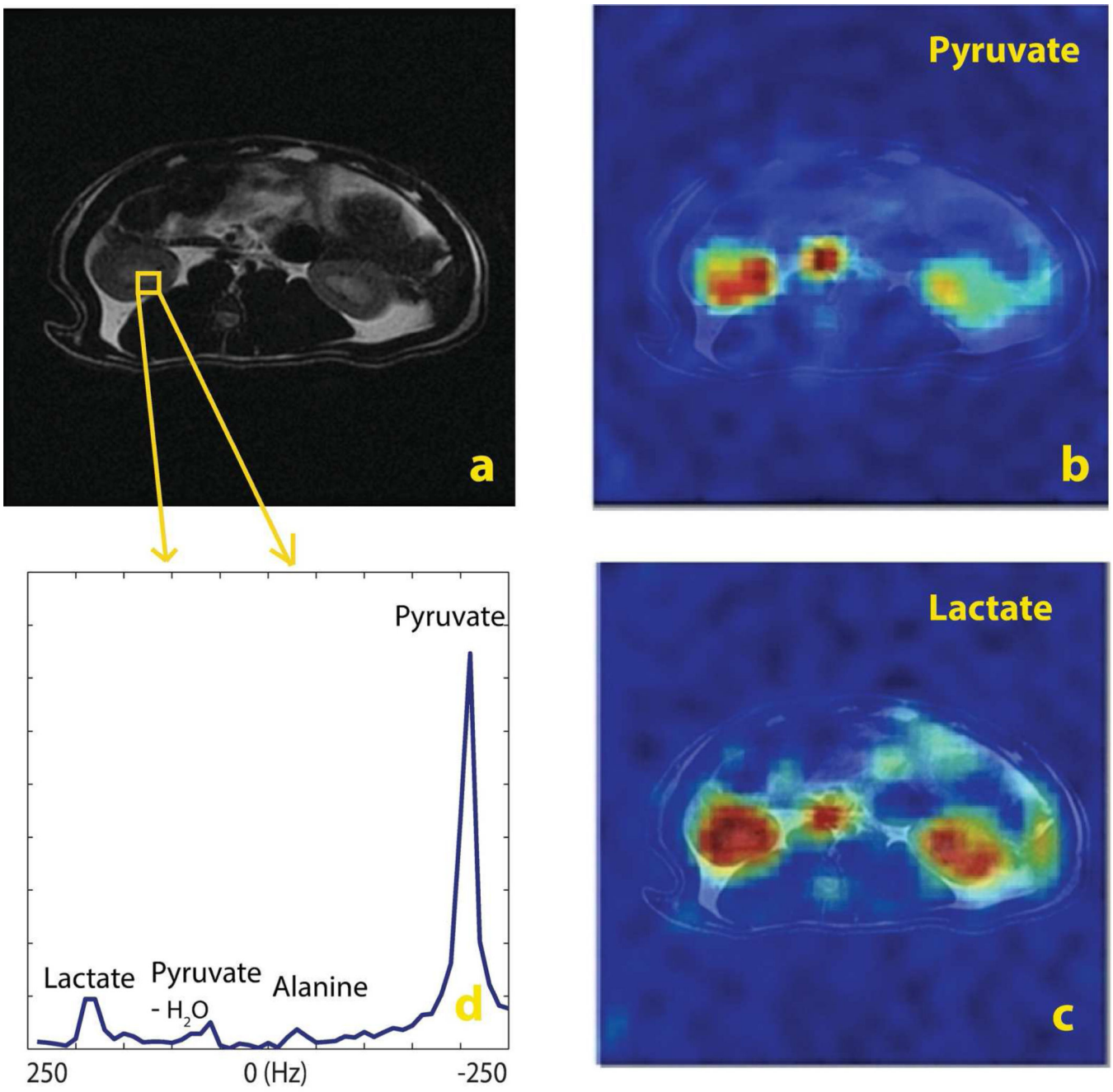

Figure 6.

In vivo results using concentric rings in a normal rat (axial): a.^{1}H T2-weighted localizer; b. [1-^{13}C] pyruvate image; c. [1-^{13}C] lactate image; d. the ^{13}C spectrum of a selected voxel with 500 Hz SBW. MRSI was acquired with a spatial resolution of 3.67×3.67 mm^2. Pyruvate and lactate images were twice zero padded to have a resolution of 1.83×1.83 mm^2. For display purposes, the intensity of lactate image was scaled up by 7. The total scan time was 2.2 s.

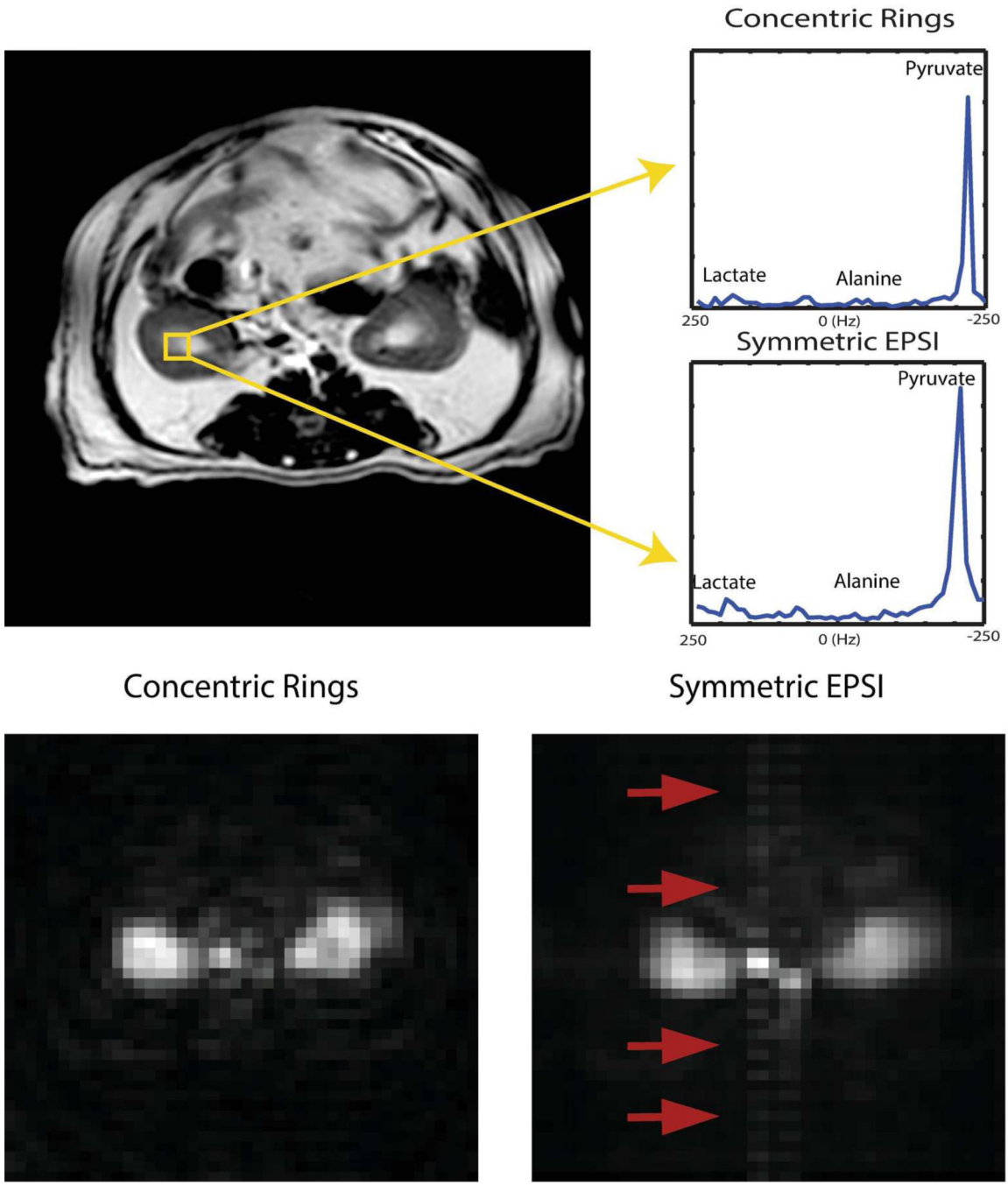

Figure 7.

In vivo results in an axial kidney slice using concentric rings and symmetric EPSI: (top-left) ^{1}H T2-weighted localizer; (top-right) spectrum from concentric rings trajectory and spectrum from EPSI trajectory respectively, both sequences captured the conversion of pyruvate with comparable SNR; Bottom figures show pulsatile flow effects on concentric rings and EPSI: (bottom-left) 2D image from the concentric rings and (bottom-right) 2D image from EPSI, via projection along spectral domain.

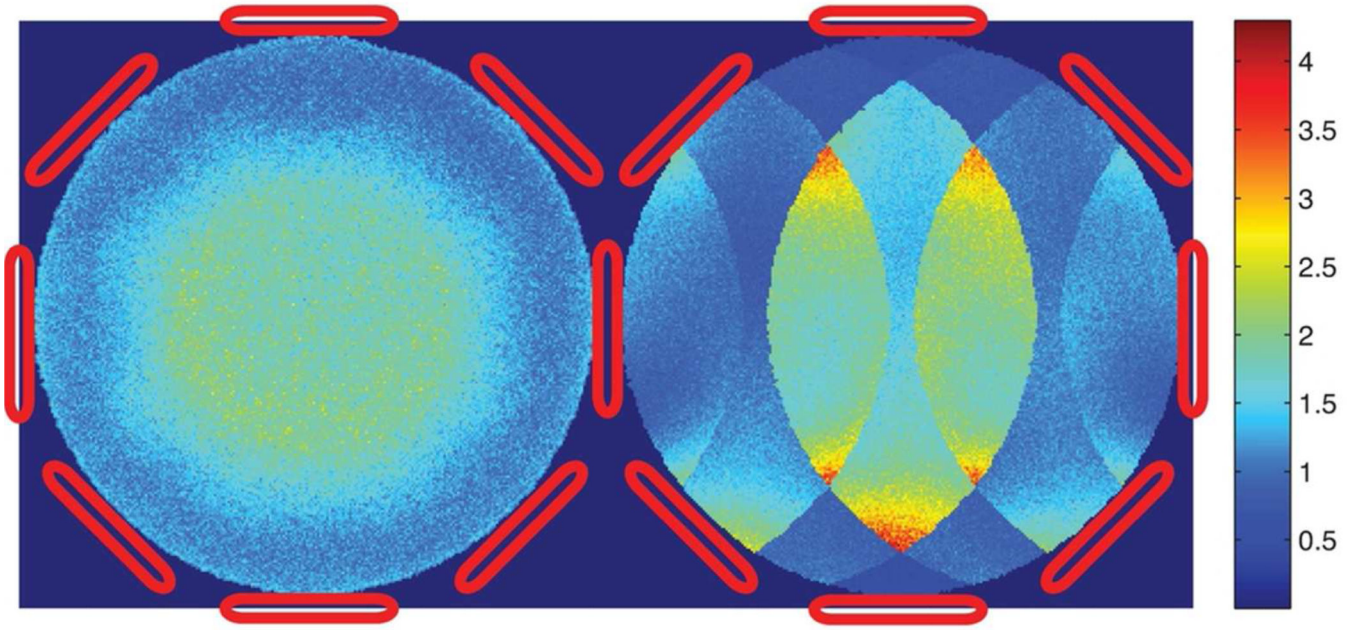

Figure 8.

Simulated g-factor map of 4× undersampled concentric rings trajectory (on the left) and Cartesian trajectory counterpart, such as EPSI, (on the right) for a simulated 8-channel array. The isotropic non-Cartesian undersampling pattern of the concentric rings trajectory results in less coherent noise amplification than the Cartesian counterpart.

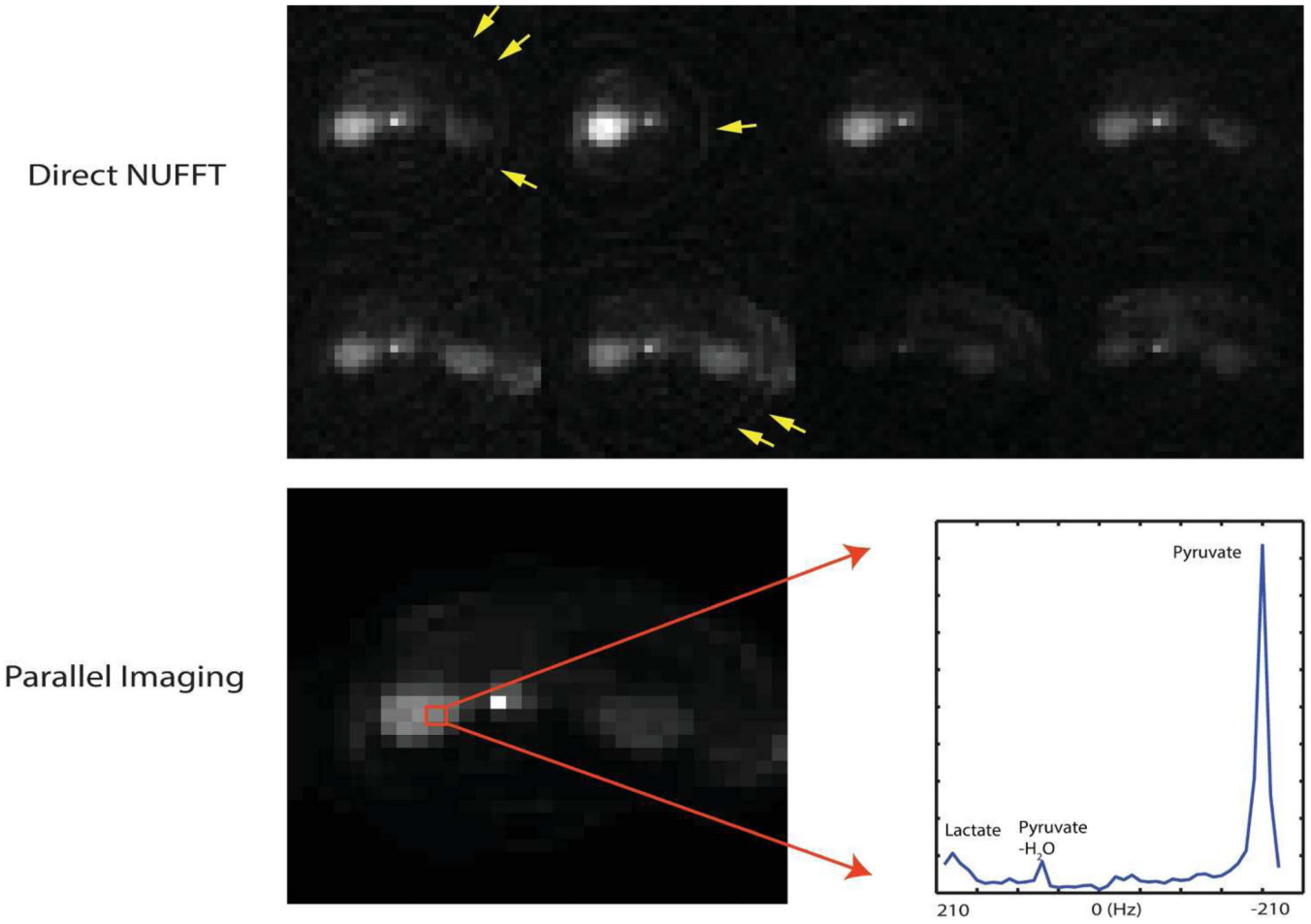

Figure 9.

Parallel imaging in vivo results in an axial kidney slice using CRT with an 8-channel phased-array rat coil: the spectroscopic imaging CRT was spatially undersampled by 1.45, with a spatial resolution of 2.5×2.5 mm^2, 8×8 cm^2 FOV and 420 Hz SBW. The top row shows individual coil images of the undersampled CRT using a direct NUFFT reconstruction, where the coil images were generated by projection along the spectral domain. The 8 coils were distributed isotropically around the animal in the axial plane. The bottom row shows the parallel imaging reconstruction result. The 2D image was obtained from projection along the spectral domain and the spectrum from a selected kidney voxel was displayed to show the resolution of various metabolites, including lactate resulting from metabolic conversion. The total scan time was 3.52 s.

Table 1

SNR comparison of CRT, Spiral and EPSI trajectories in a ^{13}C Phantom

	CRT	Spiral	EPSI
Raw SNR	44.1297±7.3599	42.0563±6.7352	69.9937±14.1840
Scan Time	1 min 50 s	1 min 15 s	3 min 40 s
Normalized SNR	36.4389	42.0563	40.8675